HHS Public Access

Author manuscript

Adv Mater Technol. Author manuscript; available in PMC 2020 January 01.

Published in final edited form as:

Adv Mater Technol. 2019 January ; 4(1): . doi:10.1002/admt.201800289.

The Unusual Properties of Polytetrafluoroethylene Enable Massive-Volume Vitrification of Stem Cells with Low-Concentration Cryoprotectants

Yuan Cao[1], **Gang Zhao**[1,*], **Fazil Panhwar**[1], **Xiaozhang Zhang**[1], **Zhongrong Chen**[1], **Lin Cheng**[2], **Chuanbao Zang**[3], **Feng Liu**[3], **Yuanjin Zhao**[4], **Xiaoming He**[5,6,7,*]

[1]Department of Electronic Science and Technology, University of Science and Technology of China, Hefei 230027, Anhui, China

[2]Department of Emergency Surgery, Qilu Hospital, Shandong University, Jinan, Shandong, China

[3]Yinfeng Cryomedicine Technology Co., LTD, Jinan, China

[4]State Key Laboratory of Bioelectronics, School of Biological Science and Medical Engineering, Southeast University, Nanjing, Jiangsu, 210096, China

[5]Fischell Department of Bioengineering, University of Maryland, College Park, MD 20742, USA

[6]Robert E. Fischell Institute for Biomedical Devices, University of Maryland, College Park, MD 20742, USA

[7]Marlene and Stewart Greenebaum Comprehensive Cancer Center, University of Maryland, Baltimore, MD 21201, USA

Abstract

Injectable stem cell-hydrogel constructs hold great potential for regenerative medicine and cell-based therapies. However, their clinical application is still challenging due to their short shelf-life at ambient temperature and the time-consuming fabrication procedure. Banking the constructs at cryogenic temperature may offer the possibility of “off-the-shelf” availability to end-users. However, ice formation during the cryopreservation process may compromise the construct quality and cell viability. Vitrification, cooling biological samples without apparent ice formation, has been explored to resolve the challenge. However, contemporary vitrification methods are limited to very small volume (up to ~0.25 ml) and/or need highly toxic and high concentration (up to ~8 M) of permeable cryoprotectants (pCPAs). Here, we show that polytetrafluoroethylene (PTFE, best known as Teflon for making non-stick cookware) capillary is flexible and unusually stable at a cryogenic temperature. By using the PTFE capillary as a flexible cryopreservation vessel together with alginate hydrogel microencapsulation and Fe_3O_4 nanoparticle-mediated nanowarming to suppress ice formation, massive-volume (10 ml) vitrification of cell-alginate hydrogel constructs with a low concentration (~2.5 M) of pCPA can be achieved. This may greatly

*Author to whom correspondence should be addressed. zhaog@ustc.edu.cn (G.Z.); shawnhe@umd.edu (X.H.).

Supporting Information

Supporting Information is available from the Wiley Online Library or from the author.

facilitate the use of stem cell-based constructs for tissue regeneration and cell based therapies in the clinic.

Keywords

PTFE; Fe_3O_4 nanoparticles; alginate hydrogel constructs; low-CPA vitrification

1. Introduction

Stem cell-hydrogel constructs as an injectable cell delivery system hold great potential for treating diabetes, cancer, neurodegenerative disorders, and cardiovascular diseases[1]. However, once the constructs are fabricated, continuous culture of the encapsulated stem cells at 37 °C is expensive and may induce uncontrolled differentiation and genetic changes[2]. In addition, the fabrication process may be time-consuming, which may lead to delay in the treatment of diseases. Therefore, banking of the constructs by cryopreservation to offer the potential of “off-the-shelf” availability for broad distribution to end-users when needed is an enabling technology for the stem cells based treatments[3].

Cryopreservation of cell-hydrogel constructs has been explored with two approaches: conventional slow freezing and vitrification. After slow freezing, the constructs usually lose their integrity, and the cell viability may be compromised, due to the mechanical and chemical damage induced by extensive ice formation outside and possibly inside the cells and constructs[4]. Besides, slow freezing requires an expensive programmable freezer, and the procedure is time-consuming[3]. Vitrification, an emerging cryopreservation method that seeks to minimize ice crystal formation altogether, may be desired for banking the cell-hydrogel constructs[5]. However, contemporary vitrification approaches require a high concentration of cell membrane permeable cryoprotectants (pCPAs) (up to ~8 M[6]), or/and ultra-rapid cooling/warming rates (up to 10^6 °C/min[7]), to inhibit both ice formation during cooling and devitrification/recrystallization during rewarming. The high concentrations of pCPAs may cause osmotic damage and biochemical toxicity that may induce uncontrolled differentiation of stem cells[8]. The high cooling/warming rates may limit the sample volume to ~0.25 ml with a few million cells[9]. However, billions of cells are usually needed for stem cells-based therapies[10]. Therefore, massive-volume vitrification of stem cells with a low concentration of CPAs (low-CPA) is desired for cryopreserving stem cell-hydrogel constructs.

In low-CPA vitrification, devitrification/recrystallization during rewarming is the most critical issue that should be addressed[11]. Recent studies have demonstrated that alginate hydrogel can suppress devitrification/recrystallization by effectively dampening the movement of water molecules[7b, 12]. However, to the best of our knowledge, alginate hydrogel facilitated vitrification was only accomplished with either high concentrations of pCPAs or limited sample volumes (up to ~0.25 ml). Low-CPA vitrification of massive volume of cell-alginate hydrogel constructs has not yet been explored.

Rapid rewarming such that ice nuclei and/or crystals have no enough time to grow before the temperatures exceed the melting point is another approach for suppressing devitrification/

recrystallization[13]. Ultrafast heat transfer for conventional vitrification method is usually achieved by minimizing the sample volume ranging from 2.5 μl for quartz microcapillaries (QMC) to 0.25 ml for plastic straws[7b, 14]. This does not satisfy the high demand of billons of cells for cell-based medicine[10a, 10b]. Therefore, it is imperative to explore a new cryopreservation vessel that can greatly expand the sample volume without compromising the heat transfer.

Recently, Fe_3O_4 nanoparticle (NP)-mediated magnetic induction heating (MIH) has been used to suppress devitrification/recrystallization and to improve the warming rate[15]. The method can also offer uniform heating to minimize the thermal stresses that may compromise the sample integrity by inducing crack formation associated with the non-uniformity[13a]. Although promising results have been obtained for vitrification with MIH, high concentrations of pCPAs were still used (4–8.4 M[15]). Moreover, the NPs have direct contact with the cells or tissues, which may cause overheating of the contacting cells and cytotoxicity ensues[16]. Furthermore, it is difficult to separate the cells from the magnetic NPs, which may not be desired for the clinical application of the cells.

To address the aforementioned challenges, a novel approach was developed to achieve low-CPA and massive-volume vitrification of cell-alginate hydrogel constructs by using multiscale biocompatible functional materials. In particular, flexible capillary made of polytetrafluoroethylene (PTFE, best known as Teflon for making non-stick cookware) that possesses exceptional stability at cryogenic temperatures[17] was employed as a flexible cryopreservation vessel. This can greatly expand the sample volumes for vitrification without compromising the heat transfer rate. Finally, the combined use of this macroscale PTFE capillary with alginate hydrogel microencapsulation and Fe_3O_4 NPs-mediated nanowarming enables low-CPA (2.5 M) and massive-volume (10 ml) vitrification of cell-alginate hydrogel constructs. This novel vitrification technology may be invaluable to facilitate the widespread use of stem cell-based constructs for tissue regeneration and cell-based therapies in the clinic.

2. Results and Discussion

2.1 Generation of alginate hydrogel constructs with controlled shape and size

The process of controllable generation of the alginate hydrogel constructs with various sizes is shown in Figure 1. Microdroplets with a core-shell configuration were generated using a tube-in-tube device with three concentric tubes. As shown in Figure 1A and Movie S1, this is achieved with the flow-focusing mechanism[18] by flowing two aqueous alginate solutions via inlets 1 and 2 (for making the core and shell of the microdroplets, respectively) together with corn oil via inlet 3. A real image of the tube-in-tube device is given in Figure 1B.

With 10 μl/min core and 25 μl/min shell flow rates, uniform constructs with an average diameter of 814, 680 and 524 μm could be fabricated using the device with high throughput by controlling the oil flow rate at 150, 300 and 600 μl/min, respectively (Figure 1C). Using this device, the encapsulation rate is approximately 500 cells per second, which is tenfold faster than that reported previously[7b]. Green fluorescent beads were suspended in the core fluid to confirm the formation of the core-shell structure of the alginate hydrogel constructs

for all the three different sizes (Figure 1D (a)-(c)). The core is fully enclosed in the shell, which may protect cells in the core from overheating by preventing their direct contact with the NPs in the solution outside the constructs[19]. This can also minimize immune response[20], and eliminate shear forces during subsequent injection[21]. Figure 1D (d)-(f) further present the size distribution of the constructs using the three different oil flow rates. Proabably due to the limited diffusion length of oxygen, nutrients, and metabolic wastes in vivo, constructs with a diameter of ~500 μm or smaller have been widely used for cell encapsulation and delivery[22]. In addition, the impact of smaller alginate constructs on cell vitrification has been well studied[7b, 12].Therefore, the constructs of 524 μm in diameter were selected for further studies.

2.2 Characterization of nanoscale, microscale, and macroscale biocompatible materials

Figure 2 presents the characterization of the multiscale materials used in this study. A representative transmission electron microscopy (TEM) image showing the nearly spherical morphology of the magnetic NPs (Fe_3O_4) is given in Figure 2A. Fe_3O_4 NPs display superparamagnetism behavior when their diameter is not much larger than 30 nm[23]. Figure 2B shows the size distribution of the synthesized Fe_3O_4 NPs in phosphate buffered saline (PBS, 1x by default) solution with an average diameter of 29.1 ± 2.1 nm, revealing superparamagnetism. The Fe_3O_4 NPs have a negatively charged surface according to the zeta potential analysis shown in Figure 2C. The saturation magnetization indicates that the Fe_3O_4 NPs have a high magnetization with a saturation value of 61.6 emu/g for each Fe_3O_4 NP (Figure 2D), which is consistent with previous studies[24].

The scanning electron microscope (SEM) images show the morphology of freeze-dried alginate hydrogel constructs both prior to and post low-CPA vitrification with Fe_3O_4 NPs (Figure 2E). Many wrinkles on inner and outer surfaces caused by the freeze-drying process can be seen, which is in accordance with previous reports[25]. More importantly, the appearance before (Figure 2E (a)-(c)) and after (Figure 2E (d)-(f)) vitrification is similar, indicating that the integrity of the alginate hydrogel constructs can be well maintained after vitrification with low-CPA. In contrast, structural damage has been reported for alginate hydrogel constructs after slow freezing[4a]. Furthermore, NPs only present on the outer surface of the constructs, suggesting that the alginate hydrogel shell could prevent the Fe_3O_4 NPs from penetrating into the core with cells (Figure 2E (g)-(i)). The uptake of NPs by cells without (W/O) and with (W/) the alginate hydrogel microencapsulation is shown in Figure 2F. Although cells without microencapsulation can take up the NPs (Figure 2F (a)), the alginate hydrogel shell can prevent cells in the core of the constructs from taking up the NPs (Figure 2F (b))[26].

Figure 2G depicts the effect of cooling (by plunging into liquid nitrogen) and warming (in 37 °C water) on the PTFE material. No evident change in the microstructure of the PTFE capillaries can be seen even after 10 freezing-thawing cycles (Figure 2G (a)-(b)). Furthermore, the stress-strain relationship of the PTFE capillaries prior to and after 10 cooling-warming cycles was obtained at a constant stretching rate of 5 mm/min using a universal material testing machine as previously reported[27]. As shown in Figure 2G (c), the stress-strain relationship is similar for the two groups. Moreover, no stress failure was

observed even when the tensile strain reached 100% for both groups, indicating that the material has excellent malleability and flexibility. There was also no significant difference in the mean values of tensile stress at the maximum load between the two groups (Figure 2G (d)). These observations indicate the unusual stability of PTFE at cryogenic temperatures, consistent with the literature[17]. This together with the excellent flexibility of PTFE prompted us to explore the use of PTFE capillary as a flexible and stable vessel for massive-volume vitrification of cells.

2.3 PTFE capillary as a flexible cryopreservation vessel

Vitrification by ultra-rapid cooling and rewarming are commonly achieved by minimizing the volume of samples (2.5–250 μl)[9b, 14]. PTFE, as a biocompatible material, has been widely used in artificial blood vessel applications [28]. Its excellent flexibility and malleability may make it possible to expand the sample volume for vitrification by combining PTFE capillary with a conformal frame to contain bio-sample for vitrification. The design of the conformal frame and its assembly with a long PTFE capillary (i.e., patterned PTFE capillary or PPC) is shown in Figure S1. Essentially, the long PTFE capillary is wrapped around the frame with predefined space between two loops of the capillary in the PPCs, to maximize the sample volume in a limited space (e.g., inside the electromagnetic coils needed for nanowarming in this study). The predefined space allows liquid nitrogen and warming water to directly contact the PTFE capillary for efficient cooling and warming, respectively. As a result, a large sample volume (e.g., 2 ml for the PPC #1, Figure S1A) can be held in the PPCs without compromising the heat transfer rate for vitrification. The images of the frame and PPC #1 are shown in Figure S1A (a)-(b). The size is designed to ensure it can be placed into electromagnetic coils with 50 ml centrifuge tube (Figure S1A(c)). Larger sample volume can be achieved by using PPC #2 with larger electromagnetic coils that can accommodate a 250 ml beaker (Figure S1B (a)-(c)). The image of PS with 0.25ml conventionally used for vitrification is shown in Figure S1C.

To evaluate the potential of the PTFE capillary as a cryopreservation vessel, the thermal profiles of the samples loaded in the PTFE capillary during cooling/warming was investigated as compared to that of PS (Figure S2). This was done by plunging the two types of cryopreservation vessels containing CPA #1 (1 M ethylene glycol or EG, 1.5 M propylene glycol or PG, 1 M trehalose, and 10% (w/v) dextran T50) into liquid nitrogen for cooling and 37 °C water bath for warming. As shown in Figure S2 A-B, the thermal profiles and the cooling and warming rates resulting from the two typles of vessels are similar, further demonstrating the feasibility of using the PPCs for vitrification.

2.4 Vitrification of stem cell-alginate hydrogel constructs

Figure 3 shows vitrification of stem cell-alginate hydrogel constructs in PPC #1 and PS with conventional water bath warming or NPs-mediated MIH. As illustrated in Figure 3A, vitrification of stem cell-alginate hydrogel constructs with PPC #1 was handled in the same way as the conventional PS. The constructs were collected and equilibrated in the CPA solutions, and the constructs were loaded in PPC #1 using syringes as shown in Figure 3A (a). Afterward, the PPC #1 was plunged into liquid nitrogen for cooling (Figure 3A (b)). Finally, the sample was warmed in a 37 °C water bath without (Figure 3A (c)-(d)) or with

(Figure 3A (e)-(f)) the MIH. For the MIH group, an alternating current (AC) magnetic field (5, 15, 25A, 375 kHz) was used. The conventional water bath warming method is soften associated with large temperature gradient and long warming time due to the limited thermal conductivity of the sample. For the MIH, owing to the Neel relaxation of the Fe_3O_4 NPs, the energy of the electromagnetic field is converted into heat[29] to achieve rapid and uniform warming[30].

Figure 3B depicts the two types of cryopreservation vessels (PPC #1 and PS) undergoing cooling in liquid nitrogen and warming in a water bath without (Figure 3B (a)) or with MIH (Figure 3B (b)). For MIH, CPA #2, consisting of CPA #1 and 0.5% (w/v) Fe_3O_4 NPs, was used. During cooling, the solution of CPA #1 in both the PPC #1 and PS can achieve vitrification (no visible ice formation). Devitrification was observed in both the PPC #1 and PS during warming without MIH, due to the very low CPA concentration used. Similarly, for the MIH group, both PPC #1 and PS can be used to achieve vitrification during cooling (Figure 3B (b), Movie S2 for PPC #1, Movie S3 for PS). With MIH during warming, devitrification appears to be mitigated (Movie S4 for PPC #1, and Movie S5 for PS). This is probably due to the enhanced heating rate (Figure S2 C-D) to reduce the time for ice to grow and the localized heating of the NPs to prevent ice nucleation next to the NPs[31].

2.5 Effect of alginate hydrogel microencapsulation and Fe_3O_4 NPs-mediated MIH on vitrification

Alginate hydrogel, which possesses desirable properties including biocompatibility, permeability, biodegradability, and mild gellation[32], has attracted tremendous attention in cell encapsulation[33]. Stem cell (including mesenchymal stem cell, MSC)-laden hydrogel constructs have extensive applications in regenerative medicine and cell therapy[34]. In previous studies, high concentration (~5–8 M) of CPAs has been used for vitrification of cell-laden constructs[35]. However, such high concentration of CPA may result in osmotic injuries and toxicity on cells in the constructs[36]. As a result, it is imperative to use multiple steps to load/unload CPA, and to optimize exposure time to the high concentration of CPAs to reduce injury. All these make the conventional vitirficaiton procedure complicated and time-consuming.

Considering the combined suppressing effect of alginate hydrogel microencapsulation and Fe_3O_4 NP-mediated MIH on ice recrystallization/devitrification, a low concentration of CPA (CPA #1, 2.5 M pCPA) was used for vitrification in this study. Viability and attachment efficiency of cells released out of the constructs and 3D culture of the constructs post-vitrification are shown in Figure 4. The constructs undergoing the addition and removal of CPA without vitrification, are used as a control. It can be seen that there is no significant difference in the viability of the MSCs in the constructs between the PPC #1 and PS group (Figure 4A and Table S1). The post-vitrification viability of the non-encapsulated cells is approximately 10% for both groups, while it reaches approximately 70% for the cells encapsulated in the constructs. This is consistent with previous studies[7b, 14], where it demonstrated that alginate hydrogel could effectively dampen the movement of water molecules to inhibit devitrification and protect the encapsulated cells from injury during the warming process.

To further suppress devitrification/recrystallization, magnetic NPs (Fe_3O_4)-mediated MIH was adopted in this study. Fe_3O_4 NPs have been approved for clinical use by the US Food and Drug Administration (FDA)[37] and have been widely explored for various biomedical application[38]. In cryopreservation, although studies have been reported on MIH aided vitrification, high concentrations of pCPAs (e.g., 4 M for cells[15a] and 8.4 M for tissues[15b]) were still used. As aforementioned, the cell viability is only ~70% when vitrifying the MSC-laden alginate hydrogel constructs with the PPC #1 at a low concentration of pCPAs (~2.5M). To obtain optimal parameters for MIH, the effect of the concentration of Fe_3O_4 NPs and current intensity were investigated (Figure 4B). It can be seen that the viability of the microencapsulated MSCs does not change significantly for 0.1% (w/v) Fe_3O_4 NPs when the current intensity varies from 5 A to 15 A and 25 A. When the concentration of Fe_3O_4 NPs is increased to 0.5% (w/v), viability of the microencapsulated MSCs significantly increases at 15 A. Nevertheless, the viability is not significantly increased at 1% (w/v) compared with that at 0.5% (w/v). Therefore, 0.5% (w/v) Fe_3O_4 NPs at 15A are considered optimal for this study. More importantly, under this optimal condition, the simultaneous use of both microencapsulation and MIH can greatly improve cell viability (more than 7 times, from 11.4% to 84.4%) (Figure 4B and Table S2). Besides, for the cells without encapsulation, their viability can be improved from 10% to 30% using 0.5% (w/v) Fe_3O_4 NPs at 15 A. It was also found that Fe_3O_4 NP-mediated MIH can significantly improve the long-term cell survival (i.e., attachment efficiency). The attachment efficiency can be improved from 0% to 4.5% without encapsulation. Strikingly, the attachment efficiency can even be improved from 0% to ~60.1% with 0.5% (w/v) Fe_3O_4 NPs at 15 A after 24 h culture for encapsulated cells (Figure 4C and Table S3). A similar effect of MIH on cell survival is observed for the PS group (Figure S3).

Figure 4D shows the typical images of live/dead (AO/EB) fluorescence staining of the cells post-vitrification under different combinations of microencapsulation and MIH. Typical differential interference contrast (DIC) images showing the cell attachment before and after vitrification in different conditions are presented in Figure 4E. The results demonstrate that the attachment efficiency after vitrification, representing the long-term viability of the cells, could be greatly improved by the combination of alginate hydrogel microencapsulation and MIH. This implies that the combination of microencapsulation and MIH may effectively suppress devitrification/recrystallization.

To further evaluate the quality of the stem cell-alginate hydrogel constructs post-cryopreservation, they were cultured for up to 7 days (Figure 4F). No significant difference was found between the fresh (Figure 4F (a)) and cryopreserved cells (Figure 4F (b)). The micrographs indicate that the cells in the constructs post-cryopreservation proliferated similarly to the fresh control cells and the integrity of microcapsules after 7 days proved the stability of the biocomposites post-vitrification.

2.6 Functional properties of microencapsulated MSCs post-vitrification

Figure 5 shows the functional evaluation of MSCs released from the constructs post-vitrification. The cell surface antigens of MSCs were analyzed by immunostaining and flow cytometry. The cells are positive for CD44 and CD90, and negative for CD45 in both fresh

and cryopreserved groups (Figure 5A). The expression of the aforementioned protein makers post-vitrification (CD44(+), CD90(+), and CD45(−)) is similar to that of fresh control cells (Figure 5B). The multilineage differentiation capacity of the cells was assessed based on osteogenic and adipogenic differentiation. As shown in Figure 5C, the adipogenic differentiation capability of the cells is confirmed by Oil red O stain of lipid vacuoles after 14 days of culture, and the calcific deposition visualized by Alizarin red S stain after 21 days demonstrates the osteogenic differentiation potential of the cells in both groups. The cells released from the constructs post-cryopreservation also have similar proliferation to the fresh control cells during three days of culture (Figure 5D). The DIC micrographs of the cells showing their morphology during 3 days of culture are given in Figure 5E. No evident difference between the cryopreservation and the fresh group is observable.

2.7 Scalability for Low-CPA vitrification with PPCs

An important advantage of our PTFE capillary-based approach for vitrification is that it can be easily scale-up, thanks to the unusual stability and flexibility of PTFE at both cryogenic and ambient temperatures that allows winding and unwinding them around the conformal frame. To demonstrate this, we conduct further experiment with PPC #2 made by winding the PTFE capillary around another design of the conformal frame with four units (Figure 6A and Figure S1B). This PPC #2 can hold 10 ml of sample for vitrification, which is 40 times larger than that of the commonly used plastic straw. A larger electromagnetic coil that could accommodate a 250 ml beaker, was utilized to warm the PPC #2. Typical images of live/dead (AO/EB) fluorescence staining of constructs W/ or W/O MIH post vitrification in PPC #2, are shown in Figure 6B. The viability of cells post vitirfication with MIH is ~84%, which is significantly higher than that without MIH (~70%, Figure 6C). The cells were further released from the constructs and their proliferation was studied during three days of culture as shown in Figure 6D. No significant difference was observed in proliferation between the post-vitrification and fresh cells (Figure 6E). These data indicate that the novel approach developed in this study can be easily scaled up to vitrify massive-volume of samples.

2.8 Possible mechanism for vitrification of the stem cell-alginate hydrogel constructs

To understand the possible mechanisms of the aforementioned low-CPA vitrification approach, cryomicroscopy experiments were performed with different combinations of CPAs, NPs, and alginate hydrogel for both cooling and warming (Figure 7). As shown in Figure 7A, a specially fabricated microdevice was used to form an alginate hydrogel slice with a thickness of 200 μm. Then, the slice with the microdevice was loaded onto the cryostage for further study. Representative micrographs showing ice formation during cooling and warming are given in Figure 7B. The end temperature for cooling was −120 °C, and the cooling/warming rate was set at 100 °C/min. The cooling and warming of CPA solution, CPA solution with Fe_3O_4 nanoparticles (CPA-NPs), and alginate hydrogel were investigated. For the CPA group, apparent ice formation manifested by spotted darkening starts at −74 °C during cooling, and the maximum crystallization appears at −99 °C during cooling. During warming, sudden darkening of the entire field of view due to recrystallization occurs at −21 °C. For the CPA-NPs group, Fe_3O_4 NPs promote the initial occurrence of ice formation at −63 °C (which is approximately 10 °C above that of the CPA

group), and the maximum crystallization appears at −68 °C (which is approximately 30 °C above that of the CPA group) during cooling. Furthermore, the total crystallization of the CPA-NPs group is greater than that of the CPA group, which is indicated by the darkness of the samples at the end of cooling. This is consistent with previous reports that NPs could effectively facilitate ice formation in CPA solution and significantly reduce supercooling of the solution by improving ice nucleation[39]. For the alginate hydrogel group, however, no visible ice crystals form during the entire cooling process, and only very tiny ice crystals can be observed during warming (at −21 °C). These results confirm that the alginate hydrogel can effectively suppress ice formation during both the cooling (ice crystallization) and warming (ice recrystallization/devitrification) processes [7b].

According to the experimental findings, a schematic showing the mechanism for vitrification of the constructs is illustrated in Figure 7C. Although no visible ice forms during cooling, devitrification/recrystallization may occur during warming for the low-CPA vitrification without alginate hydrogel microencapsulation (W/O Encap) and without MIH (W/O MIH). Devitrification/recrystallization can further trigger intracellular ice formation (IIF) in suspended cells during warming, which may result in cell death. Although the introduction of NP-mediated MIH alone can decrease devitrification/recrystallization by both more rapid global warming and local suppression of ice nucleation, it is not enough to achieve high cell viability. It is worth noting that NP-mediated MIH may cause overheating and cell death if the NPs have direct contact with cells. Similarly, although microencapsulation with alginate hydrogel alone can protect most of the encapsulated cells from IIF, some cells may still experience IIF induced by the extensive recrystallization/devitrification of water outside the microscale constructs during warming. More importantly, if the alginate hydrogel microencapsulation and NP-mediated MIH are combined, the dual inhibiting effect on devitrification/recrystallization can protect both the encapsulated cells and the construct. The decrease of the freezable water by the introduction of the alginate hydrogel and the global and local heating by the NP-mediated MIH can reduce devitrification/recrystallization outside the microscale constructs. In addition, the core-shell structure of the constructs can well protect the cells encapsulated in the core from potential overheating by avoiding direct contact with the NPs. This approach may be valuable for banking cells to facilitate their wide clinical application in cell-based medicine, although further studies are needed with other types of cells (i.e., induced pluripotent stem cells) to identify the material design principle so that the approach is applicable to many different types of cells in the future.

3. Conclusions

In this study, nanoscale (Fe_3O_4 NPs), microscale (alginate hydrogel microcapsule), and macroscale (PTFE capillary) materials are successfully combined to achieve low-CPA and massive-volume vitrification of stem cells. A tube-in-tube microfluidic device is used to produce core-shell alginate hydrogel microcapsules with cells encapsulated in their core. The use of the PTFE capillary greatly expands the sample volume without compromising the heat transfer to achieve massive-volume vitrification. The alginate hydrogels (microscale) could inhibit crystallization by effectively dampening the movement of water molecules during warming. The Fe_3O_4 NP (nanoscale)-mediated magnetic induction heating could suppress devitrification/recrystallization during warming by inhibiting ice nucleation locally

and enhancing warming globally. In addition, the alginate hydrogel shell of the microcapsules could separate stem cells from Fe_3O_4 NPs, to eliminate overheating of the cells. Cell-alginate hydrogel constructs with intact microstructure, great cell viability, and excellent biological function could be obtained with the novel massive-volume vitrification technology. Therefore, it may be valuable for banking stem cells and their constructs to meet their ever-increasing demand by modern cell-based medicine.

4. Experimental Section

Materials and Reagents:

All chemicals were obtained from Sigma (St. Louis, MO, USA) unless otherwise described. CPA #1 solution contains 1 mol/L (M) EG, 1.5 M PROH, 10% (w/v) dextran T50 (≈0.002 M), and 1 M trehalose in mother liquor. CPA #2 solution contains CPA #1 and 0.5% (w/v) Fe_3O_4 NPs. The mother liquor was composed of 80% fetal bovine serum (FBS; w/v) and 20% (w/v) culture medium.

MSCs isolation and cell culture:

Human umbilical cord blood-derived MSCs were generously provided by Xin'An Stem Cell Engineering Co., LTD (Hefei, Anhui, China). Informed consent for the donation of the MSCs used in this study was obtained prior to parturition. The isolated MSCs were cultured in DMEM (Hyclone, USA), supplemented with 10% (v/v) FBS (Hyclone, USA). The cells were incubated in a humidified atmosphere at 37 °C with 5% CO_2, for which the MSCs were seeded on 25 cm^2 culture flasks (Eppendorf, Hamburg, Germany). The medium was changed every other day till the cells reached 80–90% confluence. Later, 1×PBS (Hyclone, USA) was added to remove dead cells, followed by adding trypsin (Gibco, Carlsbad, CA, USA) to detach the cells. Detached cells were then centrifuged at 100 g for 5 min for immediate use or seeded into new culture flasks for passaging and use in future experiments. Early passages (passages 1–6) of MSCs are used in the study.

Plastic straw and PTFE capillary:

Two cryopreservation containers were used in this study: plastic straw (length: 13 mm, outer diameter: 2 mm, and inner diameter: 1.84 mm; FHK, Japan) and PTFE capillary (length: approximately 1.76 m in PPC #1 and approximately 8.9 m in PPC #2 outer diameter: 1.6 mm, and inner diameter: 1.2 mm; Haicheng Plastic, Shanghai, China). For the PTFE container, its cryogenic properties were studied after freezing in liquid nitrogen and warming in a water bath for multiple cycles. Optical fibers (Indigo Precision Optoelectronics Technology Co., Ltd. Suzhou, China) were utilized to measure the thermal history for determining the cooling and warming rates.

Fabrication of constructs using a tube-in-tube device:

The microdroplets were produced by three High-Precision Programmable Syringe Pumps (WK-101P, Nanjing Anerker Electronics Technology Co. Ltd., China) using a stainless-steel tube-in-tube device. The solutions that flowed into the three inlets were 2 wt% sodium alginate (Sangon Biotech, Shanghai, China) for Inlet 1 and Inlet 2, and corn oil for Inlet 3. The microdroplets flowed into a 6-cm dish (Eppendorf, Hamburg, Germany) with calcium

chloride solution (pH 7.2–7.4) to form alginate hydrogel constructs. Microcapsules of three different diameters (814, 680 and 524 μm) were produced by regulating the flow rates of the oil.

Synthesis and characterization of Fe_3O_4 NPs:

Fe_3O_4 NPs were synthesized by chemical co-precipitation of Fe^{2+} and Fe^{3+} ions with a molar ratio of 1:2 as follows. First, $FeCl_3{\cdot}6H_2O$ (3.60 g) and $FeCl_2{\cdot}4H_2O$ (1.33 g) were dissolved in deionized water (50 mL) at 70 °C under continuous nitrogen (N_2) flow and vigorous stirring. Second, $NH_3{\cdot}H_2O$ (15 mL) was added into the solution dropwise to react until the color of the sample turned to black, and the sample was further kept for 120 min to complete the reaction. Finally, Fe_3O_4 NPs were separated from the suspension solution by a magnet, washed with water and ethanol for three times, and dried in an oven at 80 ^oC overnight. The morphology of Fe_3O_4 NPs was characterized by transmission electron microscopy (TEM, Hitachi, Ltd., Tokyo, Japan). A DynaPro-MS800 instrument (Wyatt Technology, Santa Barbara, CA, USA) was used to determine the size of the NPs. Zeta potential measurement was performed with a Malvern Nano-ZS90 Zetasizer Nano instrument (Malvern Instruments Ltd., Malvern, UK). The magnetic properties were measured on a vibrating magnetometer (VSM, Quantum Design, Inc., San Diego, CA, USA).

Vitrification of MSC-laden constructs:

The constructs were incubated with 1 M EG and 1 M PG for 25 min and equilibrated in CPA #1 or CPA #2 for 15 min at 4 °C. Then, CPA #1 and the constructs were loaded into PPC #1 and PS by using a syringe. Afterward, the containers were sealed and then immersed in liquid nitrogen for 10 min. The container was warmed in 37 °C water bath rapidly with shaking. Finally, the constructs were gradually diluted in DMEM with 0.75 M, 0.5 M, 0.25 M and 0 M trehalose for 5 min, respectively. In the MIH group, the constructs were transferred to CPA #2. The samples were warmed in electromagnetic coils under an alternating magnetic field. In addition, the NPs were removed by a bar magnet after warming with MIH. The remaining steps were the same as aforementioned.

Characterization of alginate hydrogel:

The morphology of freeze-dried constructs before and post vitrification with MIH was analyzed by scanning electron microscopy (SEM, JEOL JSM-6390LA, Japan). In freeze-drying process, the alginate hydrogel constructs were frozen and dried at −80 °C for 4 h by using a Linkam FDCS196 cryostage (Linkam, Surrey, UK).

Characterization of PTFE material:

PTFE capillaries were cooled and warmed in liquid nitrogen and 37 °C water bath repeatedly for 10 times. A BX51 metalloscope (Olympus, Southend, England) and a scanning electron microscope were used to observe the morphologies of the PTFE material. The stress-strain relationship of the PTFE capillaries was determined by using a universal material testing machine (MTS810, MTS Systems Corporation, USA).

Magnetic induction heating (MIH):

The equipment (Shenzhen Shuangping Power Supply Technology Co., Ltd., China) for MIH consisted of a water cooling tank, a water pump (Hanjin, PHJ-750A, China), an intermediated frequency generator (SPG-10 (A)B-II) connected to two types of 6-loop coils (4.5 cm and 8.5 cm in diameter), and a 50 ml centrifuge tube/250 ml beaker in a 37 °C water bath.

Cellular uptake of NPs:

To evaluate the uptake of NPs, MSCs were seeded in 25 cm^2 culture flasks. After incubation for 24 h, the pure culture medium was replaced by culture medium containing Fe_3O_4 NPs and then incubated for 6 h. Subsequently, the culture medium (with Fe_3O_4 NPs) was removed, and the cells were washed 3–4 times with PBS. Finally, the cells were detached and fixed with 2.5% (v/v) glutaraldehyde for further TEM analysis. In the constructs group, after overnight incubation, the constructs were cultured with a culture medium containing Fe_3O_4 NPs for 6 h, and the cells were released from the constructs by immersing in 75 mM sodium citrate for 3 min and further processed as aforementioned for TEM test.

Cell viability:

The viability of cells in constructs and suspensions were assessed using a fluorescent staining kit of acridine orange/ethidium bromide (AO/EB) (KeyGen BioTECH Co., Ltd., China). The constructs were resuspended in a centrifuge tube with 50 μl of culture medium and 2 μl of staining reagent and incubated for 5 min at room temperature. With regard to non-encapsulated cells, 20 μl of cell suspensions and 1 μl of fluorescent dyes were mixed and incubated for 5 min at room temperature. Fluorescence images were obtained using an inverted microscope (Nikon Eclipse TiU, Tokyo, Japan) with a DS-Ri1 digital camera (Nikon, Japan). The dead and live cells in the images were judged by red and green fluorescence, respectively.

Cell attachment:

Cell attachment was analyzed at 1 day post-vitrification, and proliferation was observed for three days. The suspended and adherent cells were counted with a Muse Cell Analyzer (Merck Millipore, Germany) at one-day post-vitrification in 24-well plates. The attachment efficiency was calculated as the percentage of adherent cells to all cells seeded.

Cell proliferation:

For proliferation studies, the cells in 2D culture were detached from 24-well plates (Eppendorf, Hamburg, Germany) at 1 day after vitrification and seeded in three 96-well plates. Cell proliferation was evaluated by CCK-8 (Dojindo Inc., Kumamoto, Japan) assays. Each well was seeded with cells in 100 μl of culture medium. After cultured for 1, 2, or 3 days, 10 μl of CCK-8 was added to the wells. After 4 hours of incubation at 37 °C, the wells were measured with a microplate reader (Diagnostics Pasteur, Marne la Coquette, France). Fresh MSCs were studied as controls. The proliferation was calculated as the ratio of the cell number on day 2 and day 3 to the cell numbers on day 1. For 3D culture, the cell-alginate

hydrogel composites were cultured in 24-well plates, and cell number was observed at 1, 3, 5, and 7 days after vitrification.

Immunostaining:

Immunofluorescent staining was performed for three surface markers, $CD44^+$, $CD90^+$, and $CD45^-$. MSCs were seeded on sterile coverslips and incubated overnight, and then the glass coverslips were washed with PBS for three times to remove culture medium. Afterward, the coverslips were fixed with Immunol Staining Fix Solution (Beyotime, Haimen, China) at 4 °C overnight. The coverslips were then washed with PBS for three times. Non-specific binding was blocked by Immunol Staining Blocking Buffer (Beyotime, Haimen, China) by incubating samples in it for 1 h at room temperature before incubating the coverslips with primary mouse anti-human CD44 monoclonal antibody (1:100 dilution, Proteintech, Wuhan, China), purified mouse anti-pig CD90 (1:50 dilution, BD Pharmingen, USA), and purified mouse anti-human CD45 (1:50 dilution, D Pharmingen, USA) antibodies at 4 °C overnight. The MSCs were washed with PBS, and incubated in secondary antibody coupled to Alexa Fluor 488 (1:50 dilution, Thermo Fisher Scientific, USA) for 1 h in the dark. Afterward, the coverslips were washed to remove excess secondary antibody. Then, the cell nuclei were stained by using 4', 6-diamidino-2-phenylindole (DAPI, Beyotime, Haimen, China) for 10 min, and the coverslips were washed with PBS. Finally, the coverslips were imaged by an inverted fluorescence microscope.

Flow cytometry:

To analyze the expression of the three surface markers ($CD44^+$, CD90+, and $CD45^-$) with flow cytometry (BD FACSVerse, NJ, USA). The MSCs before and after vitrification were detached and washed by PBS for 3–4 times. Subsequently, MSCs were strained by CD44-FITC, CD45-FITC and CD90-FITC (1:1000, 1:500, and 1:500 dilution, respectively, Pharmingen, USA) for 2 h. Then the antibodies were removed, and MSCs were examed and analyzed by the FACS suite software.

Multilineage Differentiation:

Osteogenic and adipogenic differentiation assays were assessed using a StemPRO Osteogenesis and Adipogenesis Differentiation Kit (Gibco, Carlsbad, CA, USA). The MSCs were cultured in 24-well plates till the cells reached 60%−80% confluency. Then, the culture medium was removed, the cells were washed with PBS, and adipogenic and osteogenic differentiation media were added for further culture for 14 days and 21 days, respectively. During the culture, the medium was changed every 3 days. On the last day, the medium was removed, and the differentiated cells were washed with PBS and then fixed with 4% paraformaldehyde about 30 min. The cell nuclei were stained with DAPI, osteogenesis was analyzed by Alizarin red S, and Oil red O was used to evaluate adipogenic differentiation..

Statistical analysis:

All results are presented as the mean ± standard deviation (SD) of at least three independent experiments. The difference between groups was tested by Student's two-tailed unpaired *t*-tests. A p values less than 0.05 was considered statistically significant for all analyses.

Supplementary Material

Refer to Web version on PubMed Central for supplementary material.

Acknowledgments

This work was partially supported by grants from NSFC (Nos. 51476160) to G.Z., and NIH (R01EB012108 and R01EB023632) to X.H. This work was partially performed at the USTC Center for Micro- and Nanoscale Research and Fabrication.

References

[1]. a) Dufrane D, Goebbels RM, Gianello P, Transplantation 2010, 90, 1054 [PubMed: 20975626] b) Albani D, Gloria A, Giordano C, Rodilossi S, Russo T, D'Amora U, Tunesi M, Cigada A, Ambrosio L, Forloni G, Thescientificworldjournal 2013, 2013, 270260 [PubMed: 24459423] c) Chen G, Li J, Song M, Wu Z, Zhang W, Wang Z, Gao J, Yang Z, Ou C, Advanced Functional Materials 2017, 27, 1701798d) Nguyen DK, Son YM, Lee NE, Advanced Healthcare Materials 2015, 4, 1537 [PubMed: 25963828] e) Moshaverinia A, Chen C, Xu X, Ansari S, Zadeh HH, Schricker SR, Paine ML, Moradianoldak J, Khademhosseini A, Snead ML, Advanced Functional Materials 2015, 25, 2296. [PubMed: 26120294]

[2]. Stubban C, Katkov I, Loring JF, Wesselschmidt RL, Human Stem Cell Manual 2007, 47.

[3]. Wujie Zhang XH, Journal of Healthcare Engineering 2011, 2, 427. [PubMed: 22180835]

[4]. a) Canaple L, Nurdin N, Angelova N, Saugy D, Hunkeler D, Desvergne B, Journal of Hepatology 2001, 34, 11 [PubMed: 11211886] b) Heng BC, Yu YJ, Ng SC, Journal of Microencapsulation 2004, 21, 455. [PubMed: 15513751]

[5]. Iwatani M, Ikegami K, Kremenska Y, Hattori N, Tanaka S, Yagi S, Shiota K, Stem Cells 2006, 24, 2549. [PubMed: 16840553]

[6]. Fahy GM, Macfarlane DR, Angell CA, Meryman HT, Cryobiology 1984, 21, 407. [PubMed: 6467964]

[7]. a) Zhao G, Takamatsu H, He X, Journal of Applied Physics 2014, 115, 939b) Huang H, Choi JK, Rao W, Zhao S, Agarwal P, Zhao G, He X, Adv Funct Mater 2015, 25, 6939 [PubMed: 26640426] c) Zhao G, Fu J, Biotechnology Advances 2017, 35, 323. [PubMed: 28153517]

[8]. a) Karlsson JOM, Cravalho EG, Toner M, Journal of Applied Physics 1994, 75, 4442b) Richards M, Fong CY, Tan S, Chan WK, Stem Cells 2004, 22, 779 [PubMed: 15342942] c) Fahy GM, Wowk B, Wu J, Phan J, Rasch C, Chang A, Zendejas E, Cryobiology 2004, 48, 157. [PubMed: 15094092]

[9]. a) Kuwayama M, Theriogenology 2007, 67, 73 [PubMed: 17055564] b) Zheng Y, Zhao G, Panhwar F, He X, Tissue Engineering Part C Methods 2016, 22, 964. [PubMed: 27673413]

[10]. a) Karp JM, Teo G. S. Leng, Cell Stem Cell 2009, 4, 206 [PubMed: 19265660] b) Omori Y, Honmou O, Harada K, Suzuki J, Houkin K, Kocsis JD, Brain Research 2008, 1236, 30 [PubMed: 18722359] c) Stephen S, Andrei C, Connon CJ, Stem Cells Translational Medicine 2016, 5, 339. [PubMed: 26826163]

[11]. a) Liu BL, Mcgrath J, Mccabe L, Baumann M, Cell Preservation Technology 2002, 1, 33b) Fuller BJ, Cryo Letters 2004, 25, 375 [PubMed: 15660165] c) Rall WF, Fahy GM, Nature 1985, 313, 573 [PubMed: 3969158] d) Takahashi T, Hirsh A, Erbe EF, Bross JB, Steere RL, Williams RJ, Cryobiology 1986, 23, 103. [PubMed: 3698640]

[12]. Zhang W, Yang G, Zhang A, Xu LX, He X, Biomedical Microdevices 2010, 12, 89. [PubMed: 19787454]

[13]. a) Robinson MP, Wusteman MC, Wang L, Pegg DE, Physics in Medicine & Biology 2002, 47, 2311 [PubMed: 12164589] b) Youn JR, Song YS, Journal of Micromechanics & Microengineering 2012, 22, 115018.

[14]. He X, Park EYH, Fowler A, Yarmush ML, Toner M, Cryobiology 2008, 56, 223. [PubMed: 18462712]

[15]. a) Wang J, Zhao G, Zhang Z, Xu X, He X, Acta Biomater 2016, 33, 264 [PubMed: 26802443] b) Manuchehrabadi N, Gao Z, Zhang J, Ring HL, Shao Q, Liu F, Mcdermott M, Fok A, Rabin Y, Brockbank KG, Science Translational Medicine 2017, 9.

[16]. a) Wu X, Tan Y, Mao H, Zhang M, International Journal of Nanomedicine 2010, 5, 385 [PubMed: 20957160] b) Naqvi S, Samim M, Abdin MZ, Ahmed FJ, Maitra AN, Prashant CK, Dinda AK, International Journal of Nanomedicine 2010, 5, 983. [PubMed: 21187917]

[17]. a) Price DM, Jarratt M, Thermochimica Acta 2002, 392, 231b) Dyment J, Ziebl H, The tensile properties of some plastics at low temperatures, 1958.

[18]. a) Seo M, Paquet C, Nie Z, Xu S, Kumacheva E, Soft Matter 2007, 3, 986b) Garstecki P, Gitlin I, Diluzio W, Whitesides GM, Kumacheva E, Stone HA, Applied Physics Letters 2004, 85, 2649.

[19]. Zhao G, Liu X, Zhu K, He X, Advanced Healthcare Materials 2017, 6, 1700988.

[20]. Joki T, Machluf M, Atala A, Zhu J, Seyfried NT, Dunn IF, Abe T, Carroll RS, Black PM, Nature Biotechnology 2001, 19, 35.

[21]. Naqvi SM, Vedicherla S, Gansau J, Mcintyre T, Doherty M, Buckley CT, Advanced Materials 2016, 28, 5662. [PubMed: 26695531]

[22]. a) Wang C, Gong Y, Lin Y, Shen J, Wang DA, Acta Biomaterialia 2008, 4, 1226 [PubMed: 18434266] b) Endres M, Wenda N, Woehlecke H, Neumann K, Ringe J, Erggelet C, Lerche D, Kaps C, Acta Biomaterialia 2010, 6, 436 [PubMed: 19622399] c) Li HB, Jiang H, Wang CY, Duan CM, Ye Y, Su XP, Kong QX, Wu JF, Guo XM, Biomedical Materials 2006, 1, 42. [PubMed: 18458385]

[23]. Dobson J, Nature Nanotechnology 2008, 3, 139.

[24]. a) Fu Y, Mu M, Xiang W, Li J, Guangdong Chemical Industry 2009b) Gao F, Cai Y, Zhou J, Xie X, Ouyang W, Zhang Y, Wang X, Zhang X, Wang X, Zhao L, Nano Research 2010, 3, 23.

[25]. a) Wang Q, Zhang JP, Wang AQ, Carbohydrate Polymers 2009, 78, 731b) Hua S, Ma H, Li X, Yang H, Wang A, International Journal of Biological Macromolecules 2010, 46, 517 [PubMed: 20223260] c) Mawad D, Stewart E, Officer DL, Romeo T, Wagner P, Wagner K, Wallace GG, Advanced Functional Materials 2012, 22, 2692.

[26]. Gupta AK, Berry C, Gupta M, Curtis A, IEEE Transactions on Nanobioscience 2004, 2, 255.

[27]. a) Kawano, YoshioWang, YanqiaPalmer, Aubuchon RA, Steve R, Polímeros 2002, 12, 96b) Nielsen LE, Journal of Applied Polymer Science 1966, 10, 97.

[28]. a) Blumm J, Lindemann A, Meyer M, Strasser C, International Journal of Thermophysics 2008, 31, 1919b) Boudenne A, Ibos L, Gehin E, Candau Y, Journal of Physics D Applied Physics 2003, 37, 132c) Brown EN, Dattelbaum DM, Polymer 2005, 46, 3056.

[29]. a) Zhao DL, Zeng XW, Xia QS, Tang JT, Journal of Alloys & Compounds 2009, 469, 215b) Ma M, Wu Y, Zhou J, Sun Y, Zhang Y, Gu N, Journal of Magnetism & Magnetic Materials 2004, 268, 33.

[30]. Etheridge ML, Xu Y, Rott L, Choi J, Glasmacher B, Bischof JC, Technology 2014, 02, 229.

[31]. Liu X, Zhao G, Chen Z, Panhwar F, He X, ACS applied materials & interfaces 2018, 10, 16822. [PubMed: 29688697]

[32]. a) Sun J, Tan H, Materials 2013, 6, 1285 [PubMed: 28809210] b) Li Y, Rodrigues J, Rodrigues J, Tomás H, Chemical Society Reviews 2012, 41, 2193. [PubMed: 22116474]

[33]. a) Workman VL, Tezera LB, Elkington PT, Jayasinghe SN, Advanced Functional Materials 2014, 24, 2648 [PubMed: 25411575] bGhidoni I, Chlapanidas T, Bucco M, Crovato F, Marazzi M, Vigo D, Torre ML, Faustini M, Cytotechnology 2008, 58, 49 [PubMed: 19002776] c) Cheng Y, Zhang X, Cao Y, Tian C, Li Y, Wang M, Zhao Y, Zhao G, Applied Materials Today 2018, 13, 116.

[34]. a) Benoit DS, Schwartz MP, Durney AR, Anseth KS, Nature Materials 2008, 7, 816 [PubMed: 18724374] b) Williams CG, Kim TA, Malik A, Manson P, Elisseeff J, Tissue Engineering Part A 2003, 9, 679.

[35]. a) Wu Y, Yu H, Chang S, Magalhães R, Kuleshova LL, Tissue Engineering 2007, 13, 649 [PubMed: 17362134] b) Kuleshova LL, Wang XW, Wu YN, Zhou Y, Yu H, Cryo Letters 2004, 25, 241. [PubMed: 15375435]

[36]. Zhang X, Catalano PN, Gurkan UA, Khimji I, Demirci U, Nanomedicine 2011, 6, 1115. [PubMed: 21955080]

[37]. Wang J, Chen Y, Chen B, Ding J, Xia G, Gao C, Cheng J, Jin N, Zhou Y, Li X, International Journal of Nanomedicine 2010, 5, 861. [PubMed: 21042548]

[38]. a) Zeng H, Sun S, Advanced Functional Materials 2009, 18, 391b) Ninjbadgar T, Brougham DF, Advanced Functional Materials 2015, 21, 4769c) Zhao X, Zhao H, Chen Z, Lan M, Journal of Nanoscience & Nanotechnology 2014, 14, 210. [PubMed: 24730260]

[39]. Han X, Ma H, Wilson C, Critser JK, Cryobiology 2007, 55, 326.

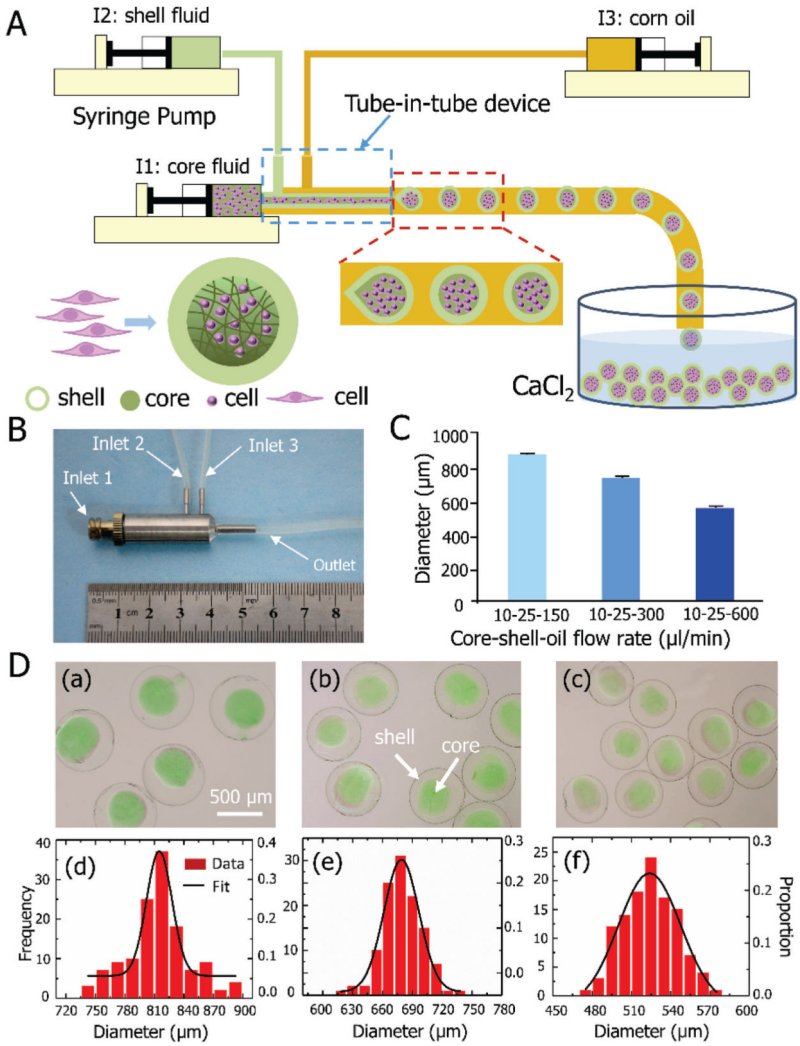

Figure 1.

Controlled generation of core-shell structured alginate hydrogel constructs. A) A schematic illustration of the construct production in a tube-in-tube device. B) Image of the stainless-steel tube-in-tube device with three inlets and one outlet. C) Average size of the constructs generated by the device with three different flow rates of oil. D) Morphology and size distribution of the constructs: (a)-(c) present the merged differential interference contrast (DIC) and fluorescence images showing the core-shell morphology and controllable size of the constructs embedded with fluorescent beads at three different oil flow rates: (a) 150, (b) 300, and (c) 600 μl/min; and (d)–(f) show the size distribution of the constructs produced under the three different flow rates of oil shown in (a)-(c). The core and shell flow rates are the same as that shown in panel C (n = 116–131).

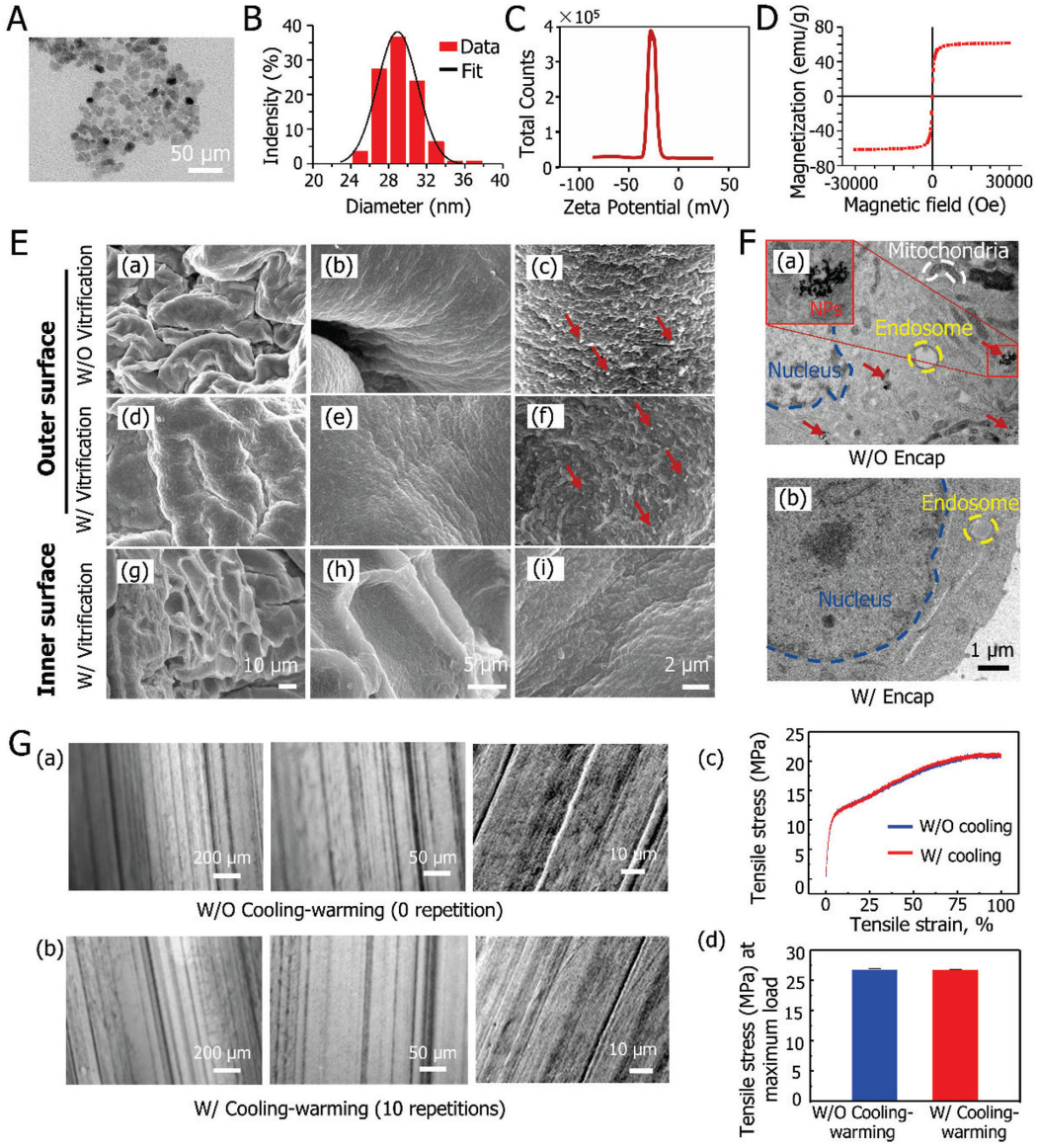

Figure 2.

Characterization of nanoscale, microscale and macroscale materials: A) TEM image of Fe_3O_4 NPs. B) Size distribution of the Fe_3O_4 NPs. C) Zeta potential of the Fe_3O_4 NPs. D) The magnetic property of the NPs. E) The morphology of freeze-dried alginate hydrogel constructs before and after low-CPA vitrification: (a)-(c) the outer surface of constructs before vitrification at different magnifications. (d)-(f) the outer surface of constructs after vitrification with NPs-mediated MIH at different magnifications, and (g)-(i) the inner surface of constructs after vitrification at different magnifications. F) TEM analyses of cells for observing NPs inside cells: TEM images of non-encapsulated (a) and encapsulated cells (b) after 6 hours of co-cultured with Fe_3O_4 NPs. G) Mechanical properties of PTFE capillary: (a)-(b) the morphology of PTFE capillaries before (a) and after (b) cooling and warming repeatedly for 10 times. (c) typical stress-strain curves of PTFE capillary without (W/O) and with (W/) cooling-warming repeatedly for 10 times and (d) the mean values of tensile stress

at maximum load W/O and W/ cooling-warming repeatedly for 10 times. Red arrows indicate NPs.

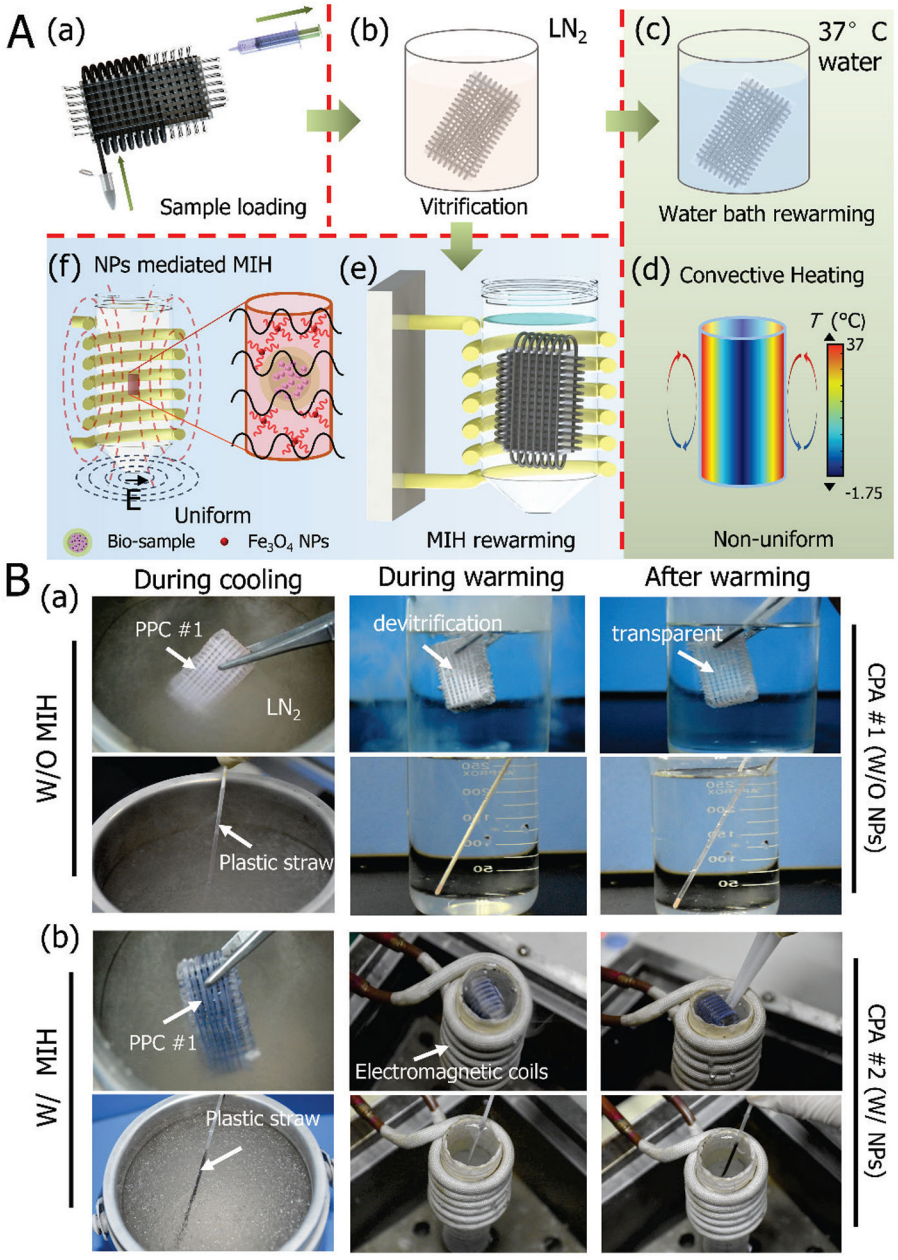

Figure 3.

Vitrification of samples in PPC #1 and PS either without (i.e., in a conventional water bath) and with magnetic induction heating (MIH) for warming. A) Schematic illustration of the procedures for vitrifying samples with PPC #1 either without or with MIH: (a) loading sample into PPC #1, (b) cooling the sample in liquid nitrogen, (c) warming the sample in a 37 ^{o}C water bath, (d) the non-uniform nature of convective heating in a water bath; (e) magnetic NPs-mediated MIH; and (f) the uniform global and local heating of MIH. B) Images taken during the cooling-warming processes using a plastic straw and PPC #1: (a) conventional heating in 37 °C of water, and (b) NP-mediated MIH.

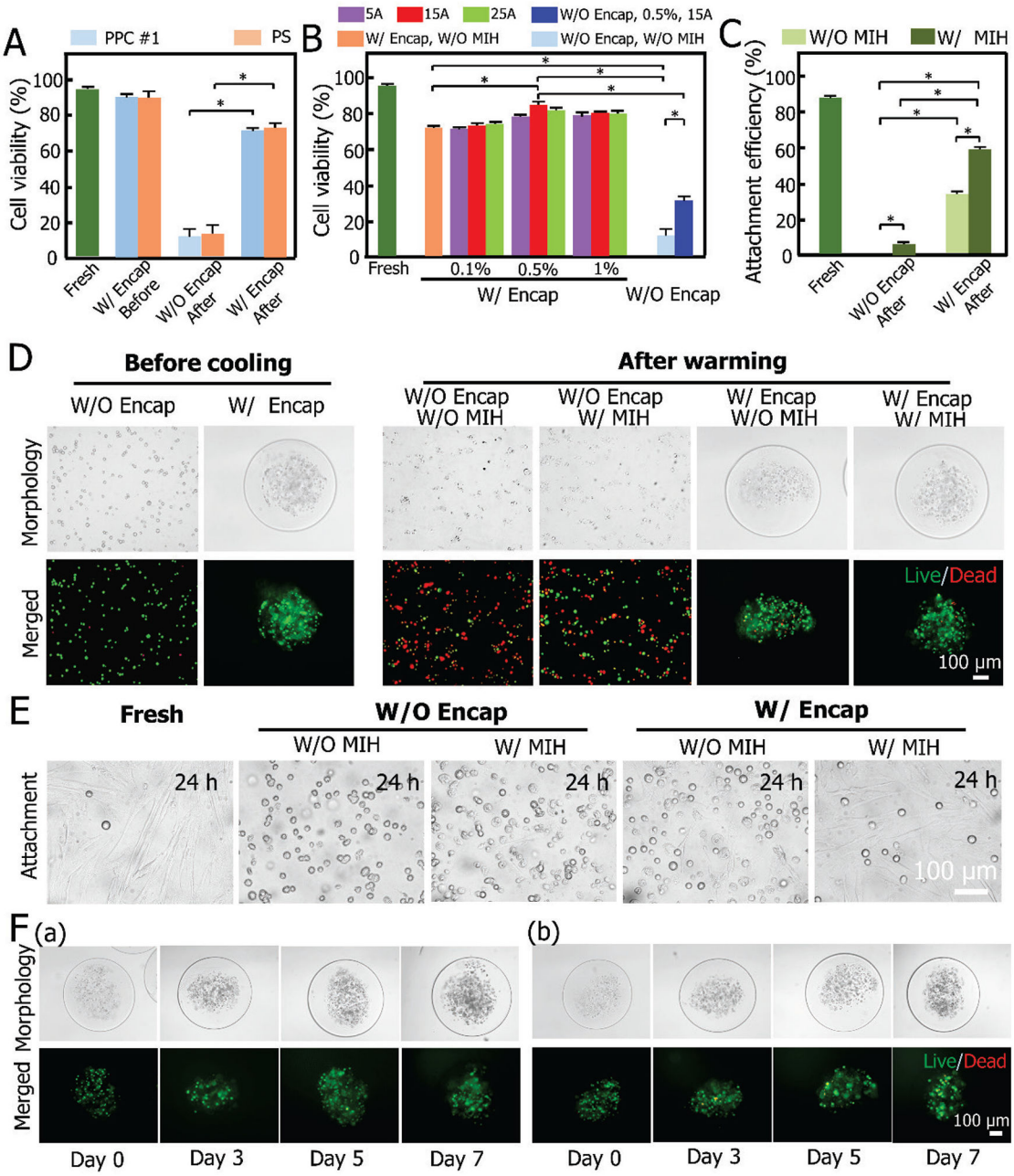

Figure 4.

Viability and attachment efficiency of the cells released from the constructs, and 3D culture of the intact constructs post-vitrification. A) Viability of MSCs in constructs either W/ or W/O encapsulation (Encap) before and after vitrification with PPC #1 and PS. *: $p < 0.05$. B) Viability of MSCs W/ or W/O (MIH and Encap) post-vitrification with PPC #1 under different conditions, i.e., 0.1%, 0.5% and 1% (w/v) Fe_3O_4 NPs with MIH under a magnetic field (5, 15, and 25 A). C) Attachment efficiency of MSCs W/ or W/O (MIH and Encap) before and after vitrification with PPC #1. D) DIC and fluorescence images showing the viability of MSCs pre- and post-vitrification using PPC #1 W/ or W/O (Encap and MIH). E) Typical DIC images are showing the attachment efficiency under various conditions. F)

Typical DIC and fluorescence images are showing the morphologies of fresh (a) and vitrified (b, with MIH and Encap) constructs and the viability and proliferation of MSCs under 3D culture in the constructs on days 0, 3, 5, and 7.

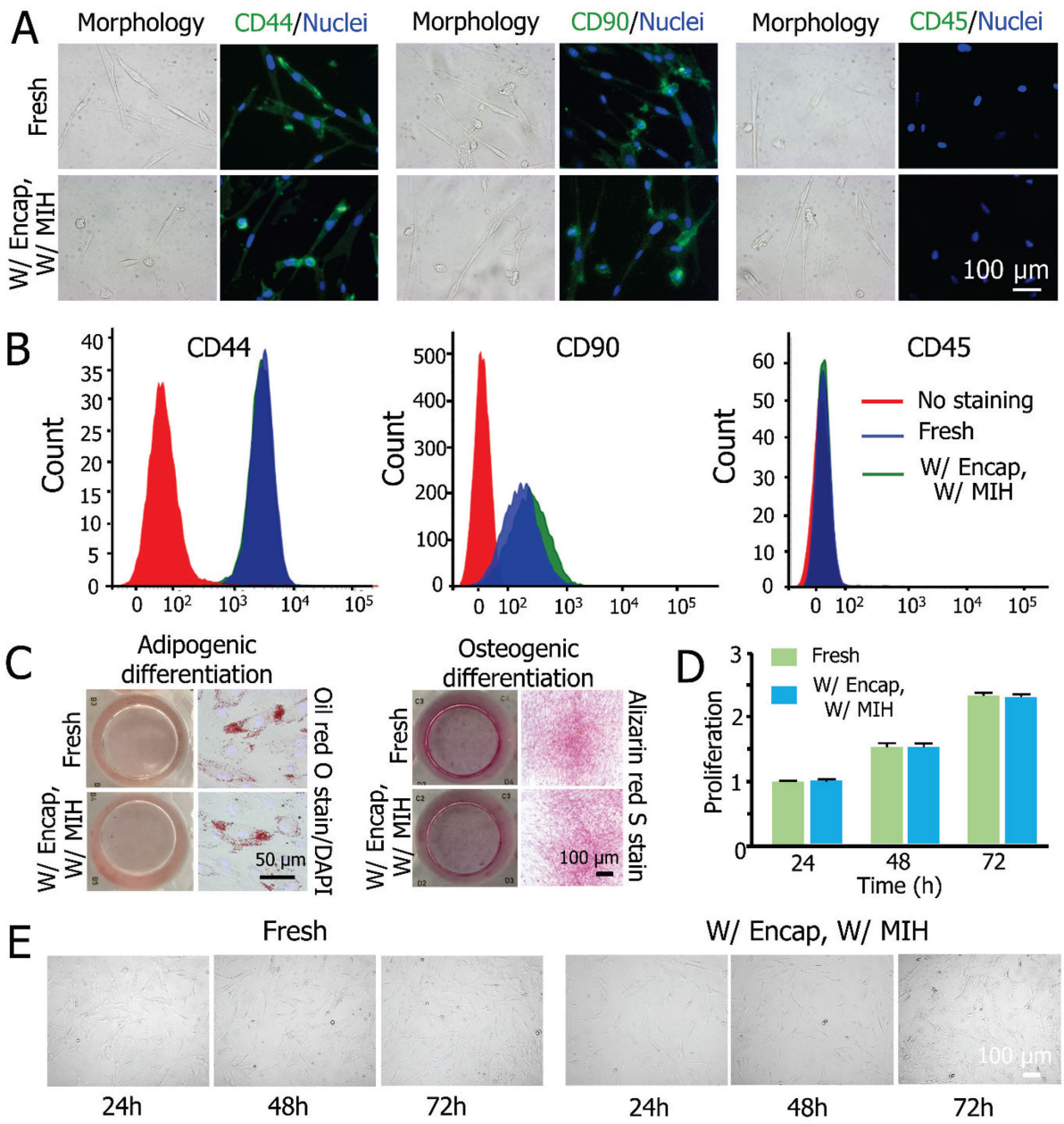

Figure 5.

Functional properties of MSCs before and after vitrification with MIH and encapsulation. A) Fluorescence immunostaining for CD44 (+), CD90 (+), and CD45 (−) showing the expression of the three markers on MSCs. B) Quantification of CD44 (+), CD90 (+), and CD45 (−) expression on the cells by flow cytometry. C) Qualitative analysis of adipogenic (left) and osteogenic (right) differentiation of MSCs post-vitrification compared to fresh cells. D) Proliferation of MSCs released from constructs post-vitrification compared to fresh cells. E) Typical DIC micrographs between cryopreserved and fresh MSCs showing the cell proliferation.

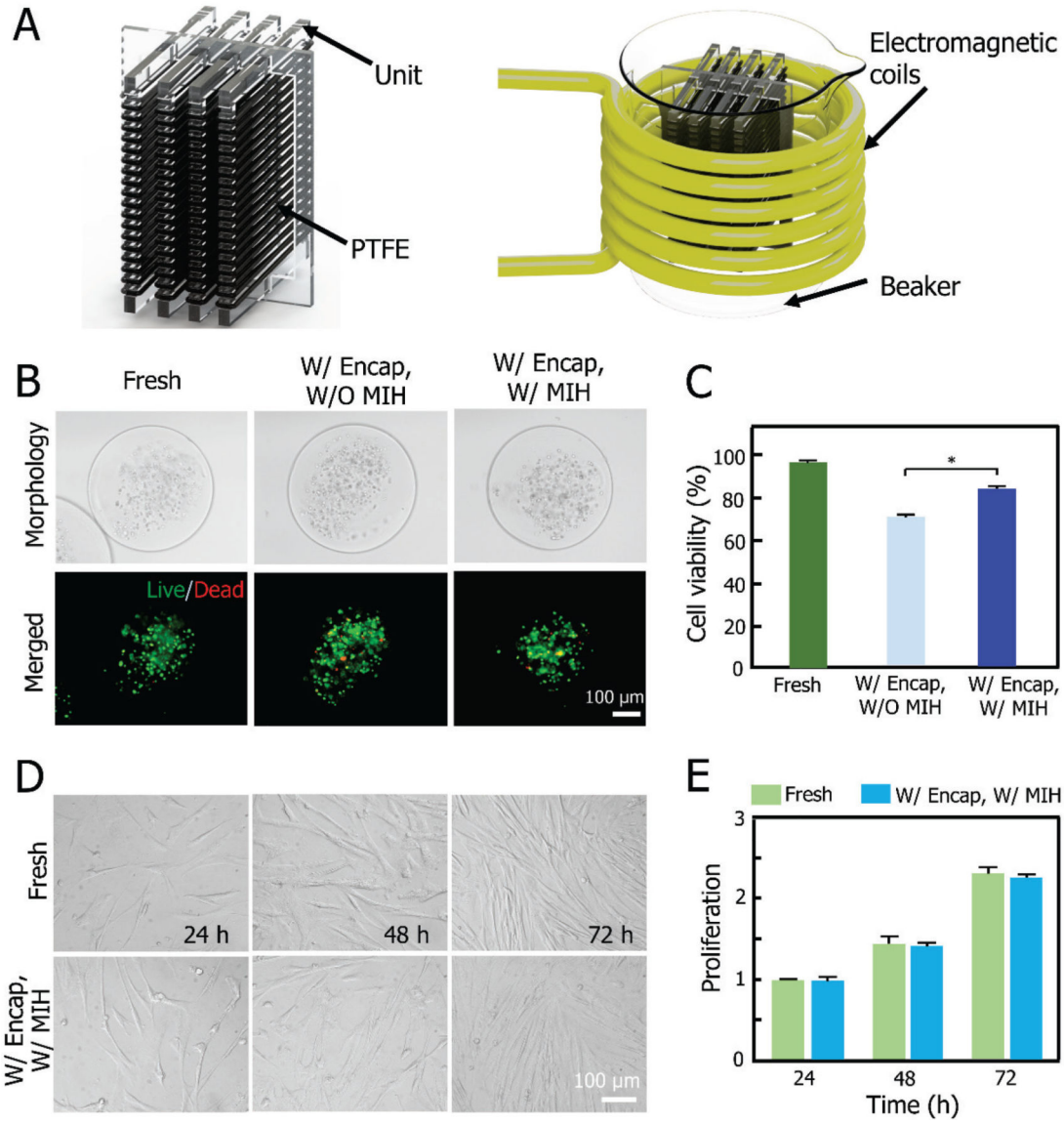

Figure 6.

Scalability of the PTFE-based technology for vitrification of cell-alginate hydrogel constructs. A) Schematic illustration of PPC #2 and the warming of PPC #2 in electromagnetic coils under alternating current (AC) magnetic field. B) DIC and fluorescence images showing the viability of constructs before and after vitrification using PPC #2 W/ or W/O MIH. C) Viability of constructs W/ or W/O MIH before and after vitrification. D) Typical DIC micrographs of the proliferation of MSCs during three days before and after vitrification with PPC #2. E) Proliferation results of MSCs before and after vitrification.

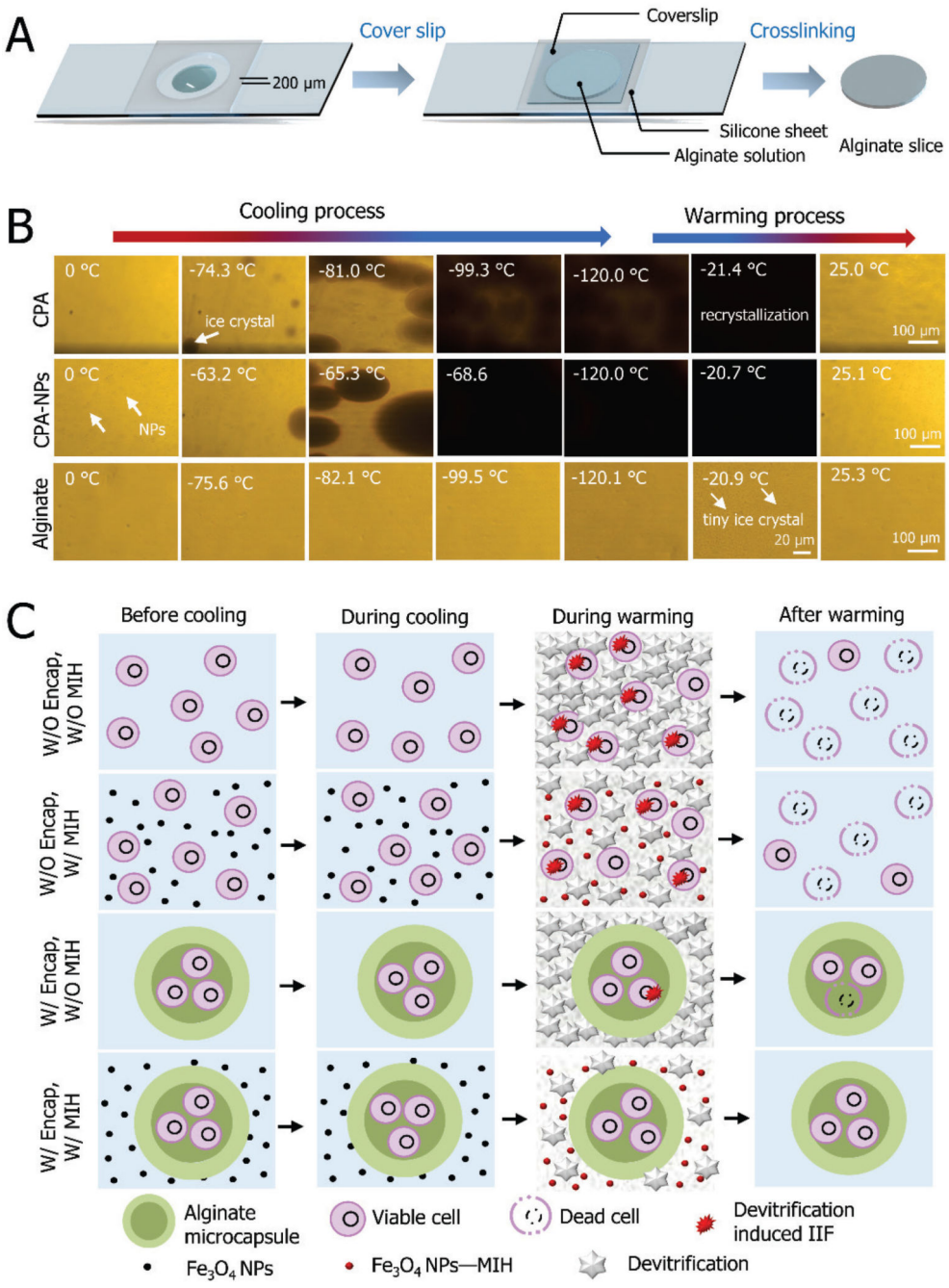

Figure 7.

The possible mechanisms of low-CPA vitrification developed in this study. A) The fabrication of alginate hydrogel slices. B) Morphological observations of ice formation in either CPA #1 and CPA #2 or in the alginate hydrogel slice without any CPA during cooling and warming. C) A schematic illustration on how alginate hydrogel microencapsulation and MIH might enhance low-CPA vitrification of cells and constructs.